LARGE-EDDY SIMULATION OF TAYLOR-COUETTE FLOW AT RELATIVELY HIGH REYNOLDS NUMBERS

D. I. Pullin
Graduate Aerospace Laboratories.
California Institute of Technology
Pasadena CA 91125, USA
dpullin@caltech.edu

Wan Cheng and Ravi Samtaney
Mechanical Engineering, Physical Science and Engineering Division
King Abdullah University of Science and Technology
Thuwal, Saudi Arabia
wan.cheng@kaust.edu.sa,ravi.samtaney@kaust.edu.sa

ABSTRACT

We discuss large-eddy simulations (LES) of the incompressible Navier-Stokes equations for Taylor-Couette flow. The ratio of the two co-axial cylinder diameters is $\eta = r_i/r_o = 0.909$ with r_i the inner cylinder radius and r_o the outer radius. The outer cylinder is stationary while the inner cylinder rotates with constant angular velocity ω_i. Subgrid stresses are represented using the stretched-vortex model (SVM) where the subgrid motion is modeled by subgrid vortices undergoing stretching by the local resolved-scale velocity- gradient field. We report wall-resolved LES at $Re_i = dr_i\omega_i/\nu$ up to $Re_i = 10^6$ with ν the kinematic viscosity of the Newtonian fluid and $d = r_o - r_i$ the cylinder gap. The present study focuses on the wall-turbulence behavior at relatively high Re_i. Comparisons are made with direct numerical simulations (DNS) and with experimental results.

1 INTRODUCTION

Taylor-Couette (TC) flow of a viscous fluid in the annular gap between two concentric cylinders, where one or both cylinders are rotating, is a classical turbulent flow that exhibits interesting shear-flow phenomena (Taylor, 1923; Grossmann *et al.*, 2016). TC flow is rather more experimentally accessible than the related plane-Couette (PC) flow owing to the cylindrical geometry and the convenience of torque measurement. TC flow can be generated in the laboratory at relatively large Reynolds numbers and over a range of parameters that include η, Reynolds number and the rotational speeds of both cylinders.

In PC flow the existence of extremely large structures presents challenges for Direct numerical simulation (DNS). The DNS studies of Pirozzoli *et al.* (2014) achieved $Re_\tau \approx 1000$ on a commonly accepted domain of $(9\pi, 1, 4\pi)$ in the unit of d which is the gap between two plates. For TC flow, if Re_i is sufficiently large, the wavelength of the Taylor rolls does not significantly influence the turbulent statistics (Ostilla-Mónico *et al.*, 2015). DNS of TC flow utilizing a small azimuthal and spanwise sector of the two concentric cylinders containing two Taylor-rolls have been reported by Ostilla-Mónico *et al.* (2016) with $Re_\tau \approx 4200$. Some turbulence features of TC flow at high Re_τ are similar to PC flow, and also to other canonical flows such as turbulent channel flow.

Re_i	N_θ	N_r	N_y	Ta
1×10^5	256	256	512	1.34×10^{10}
3×10^5	512	512	768	1.21×10^{11}
6×10^5	512	512	768	4.83×10^{11}
1×10^6	1024	1024	1024	1.34×10^{12}

Table 1. LES flows at varying Re_i. For all cases, the domain size is a sector of $\pi/10$ in the azimuthal θ direction and is $2\pi d/3$ in the spanwise y direction.

Presently we investigate Taylor-Couette flow at relatively large Reynolds numbers using the numerical technique of large eddy simulation (LES). Our aim in part is to provide data at larger Re_i than available from present DNS as a prelude to wall-modeled LES at even larger Re_τ.

2 Numerical method and physical models

2.1 Numerical method

The governing equations for LES of incompressible viscous flow are derived by formally applying a spatial filter onto the Navier-Stokes equation. These are

$$\frac{\partial \widetilde{u}_i}{\partial t} + \frac{\partial \widetilde{u}_i\widetilde{u}_j}{\partial x_j} = -\frac{\partial \widetilde{p}}{\partial x_i} + \nu\frac{\partial^2 \widetilde{u}_i}{\partial x_j^2} - \frac{\partial T_{ij}}{\partial x_j}, \quad \frac{\partial \widetilde{u}_i}{\partial x_i} = 0, \quad (1)$$

where x_i, $i = 1,2,3$ are Cartesian coordinates with $\widetilde{u}_i$ the corresponding filtered velocity and $\widetilde{p}$ the filtered pressure.

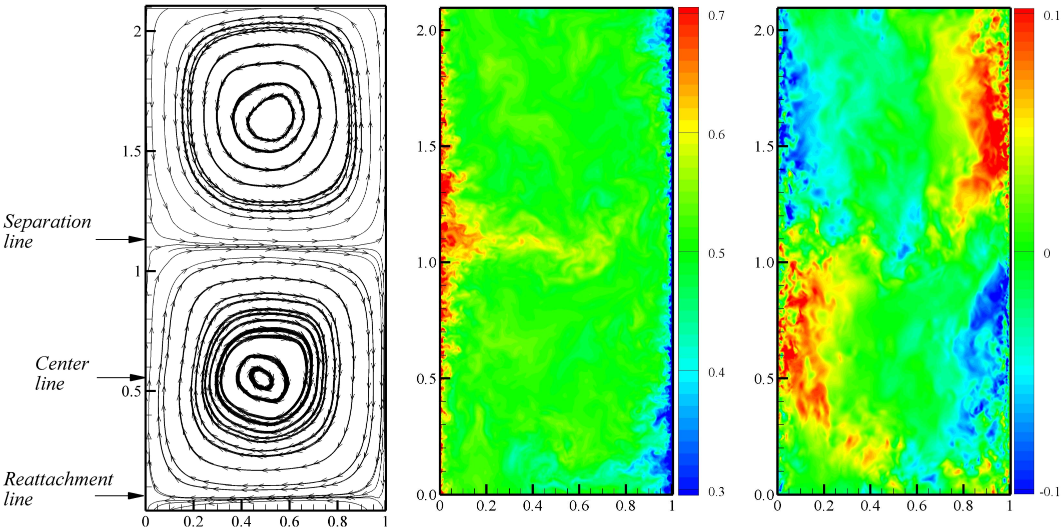

Figure 1. Visualization of an instantaneous flow field for $Re_i = 10^5$. Left: streamlines of the azimuth-averaged flow field (u_r, u_y); middle: instantaneous azimuthal velocity field at mid-span plane; right: instantaneous spanwise velocity field at mid-span plane.

$T_{ij} = \widetilde{u_i u_j} - \widetilde{u}_i \widetilde{u}_j$ denotes the effect of unresolved scales on the resolved-scale motion, which is represented using a subgrid-scale (SGS) model. We will use (x, y, z) as Cartesian coordinates with (u, v, w) as the corresponding filtered velocity components. Two other coordinate systems are also utilized; the first is cylindrical coordinates (θ, y, r) with velocity components (u_θ, u_y, u_r) which is useful for analyzing results while the second is general curvilinear coordinates (ξ, y, η) used for the implementation of the numerical method.

The governing LES equations are discretized on a body-fitted computational domain (ξ, y, η) which is mapped from the physical domain in (x, y, z) co-ordinates. A fully staggered strategy is employed for velocity components, with both physical velocity components u, w and their contravariant components u_θ, u_r computed on ξ and η faces. Spatial discretization employs a fourth-order-accurate, central-difference scheme for all terms, except the convective term which uses a fourth-order energy-conservative scheme for the skew-symmetric form (Morinishi *et al.*, 1998). For time integration, we utilize a fully implicit scheme for viscosity terms and an Adam-Bashforth method for the convective term, combined with the fractional-step method. The modified Helmholtz equation for velocity and the Poisson equation for pressure are solved with a multigrid method with line-relaxed Gauss-Seidel smoothers.

2.2 Physical model

For LES we employ the stretched-vortex SGS model (SVM) (Misra & Pullin, 1997; Voelkl *et al.*, 2000; Chung & Pullin, 2009), where the subgrid flow is modeled by spiral vortices (Lundgren, 1982) stretched by the eddies comprising the local resolved-scale flow. Generally, the SGS terms are computed on an η face, which minimizes the requirement of ghost values for implementation of wall boundary conditions. A consistent fourth-order central difference scheme is used to derive SGS terms that incorporate ghost points, via computing an additional set of SGS terms at the first above-wall center point. The present LES is "wall-resolved" meaning that the wall-normal grid size at the wall is of order the local viscous wall scale u_τ/ν where $u_\tau \equiv \sqrt{|\tau_w|/\rho}$ is the friction velocity with $|\tau_w|$ the magnitude of the wall shear stress and ρ the constant fluid density.

2.3 Cases implemented

Taylor-Couette flow is characterized by two concentric cylinders. Most generally, the inner cylinder has radius r_i and rotates with angular velocity ω_i, while the outer cylinder of radius r_o rotates with angular velocity ω_o. For the present study the outer cylinder is stationary; $\omega_o = 0$. Two typical dimensionless parameters for TC flow with an stationary outer cylinder are the radius ratio $\eta = r_i/r_o$ and the inner Reynolds number $Re_i = dr_i\omega_i/\nu$. Here $d = r_o - r_i$ is the gap between two cylinders, and ν is the kinetic viscosity of the fluid. We use fixed $\eta = r_i/r_o = 0.909$ and vary only Re_i.

In LES implementation in the sense of cylindrical (r, θ, y) co-ordinates, the computational domain is a sector of angle $\pi/10$ in the θ-direction. The spanwise domain length is $L_y = 2\pi d/3$. Periodic boundary conditions are implemented in both θ and y. Grid spacing is uniform in both the θ and spanwise y-directions but is stretched in the r direction.

The present study focuses on the wall turbulence behavior at relatively high Re_i. For numerical verification we utilize DNS Re_i at 10^5 and 3×10^5 (Ostilla-Mónico *et al.*, 2016). Higher Re_i at 6×10^5 and 10^6 are also presented. For the four cases implemented, we list the mesh size (N_θ, N_r, N_y) in table 1. The Taylor number, which for $\omega_0 = 0$ is

$$Ta = \frac{(1+\eta)^6}{64\,\eta^6} Re_i^2 \approx 1.34 Re_i^2, \tag{2}$$

is also listed in Table 1.

For defining averages the flow is assumed to be statistically stationary in time and spatially homogeneous in the θ direction only. The flow is non-homogenous in the

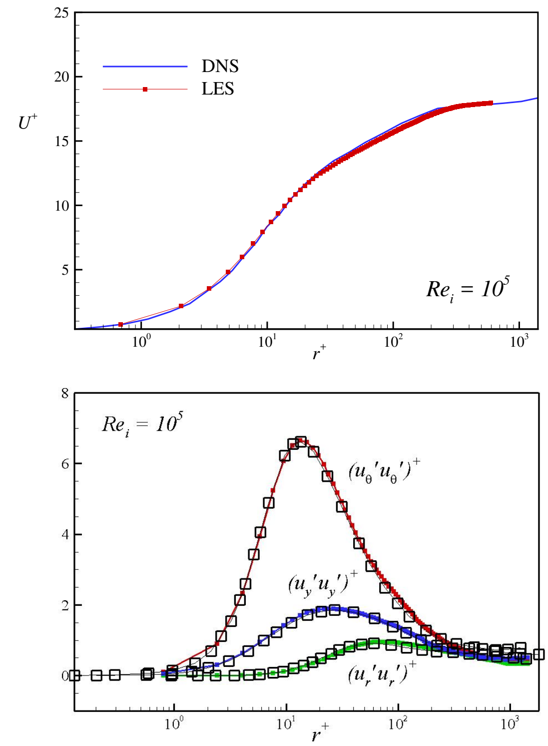

Figure 2. Comparison of TC flow at $Re_i = 10^5$. Top; mean flow velocity profiles U^+; Bottom; turbulent intensities $(u'_\theta u'_\theta)^+, (u'_y u'_y)^+, (u'_r u'_r)^+$ square symbols: DNS by Ostilla-Mónico *et al.* (2016). Solid lines with filled squares: present LES.

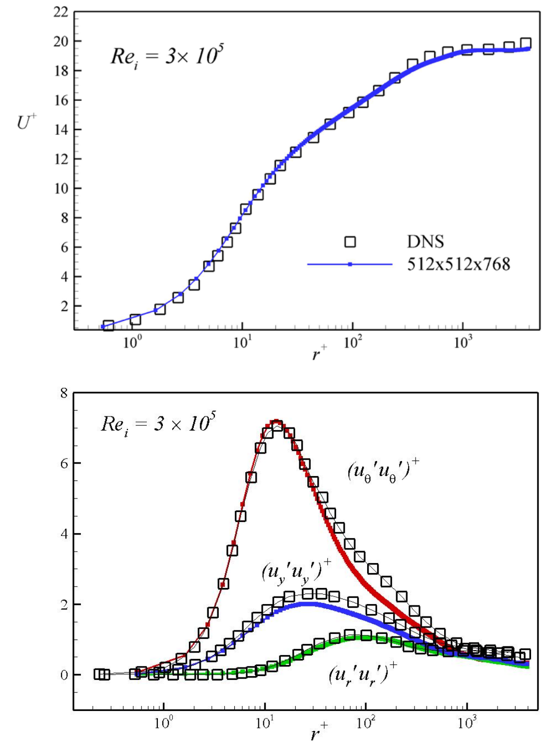

Figure 3. Comparison of TC flow at $Re_i = 3 \times 10^5$. Top; mean flow velocity profiles U^+; Bottom; turbulent intensities $(u'_\theta u'_\theta)^+, (u'_y u'_y)^+, (u'_r u'_r)^+$ square symbols: DNS by Ostilla-Mónico *et al.* (2016). Solid lines with filled squares: present LES.

spanwise direction owing the Taylor-roll structure. In what follows " $\hat{.}$" will denote an average of a space-time dependent quantity in both time and the azimuthal (θ) direction, while "$\bar{.}$ " denotes an additional spanwise average. In particular the time-azimuthal average of the velocity $\mathbf{u}(\theta, y, r, t)$ is written as $\hat{\mathbf{U}}(y, r)$ while its further spanwise average is $\overline{\mathbf{U}}(r)$. Averages of fluctuating velocity components correspondingly can have two different definitions. The first is $\mathbf{u}' = \mathbf{u}(\theta, y, r, t) - \hat{\mathbf{U}}(y, r)$, while the second is $\mathbf{u}^+ = \mathbf{u}(\theta, y, r, t) - \overline{\mathbf{U}}(r)$. Thus the turbulent statistics also can be shown in different form where $\overline{\mathbf{u}'\mathbf{u}'}$ is considered to capture only small scale turbulent motions, while $\overline{\mathbf{u}^+\mathbf{u}^+}$ also includes the effect of large-scale Taylor roll motion. In present study, for the most part we consider the radial profiles of velocity $\overline{U_\theta}(r)$ and of turbulent intensities $\overline{u'_\theta u'_\theta}$, $\overline{u'_y u'_y}$ and $\overline{u'_r u'_r}$ at different Re_i but also show some distributions of $\hat{U}_\theta(y, r)$ at different spanwise locations.

3 Comparison with DNS: $Re_i = 10^5, 3 \times 10^5$

Numerical verification is implemented via comparison with DNS by Ostilla-Mónico *et al.* (2016) at two Reynolds numbers, $Re_i = 10^5$ and $Re_i = 3 \times 10^5$. The latter is the highest Reynolds number in their DNS. Comparisons mainly include mean velocity profiles and also turbulent intensities.

In figure 1, we show some snapshot diagnostics of the flow field at $Re_i = 10^5$ viewed in an $(r - y)$ or radial-spanwise plane. Coordinates are scaled using the cylinder gap d. In the r direction $(r - r_i)/d = 0$ corresponds to the inner, rotating cylinder and $(r - r_i)/d = 1.0$ to the outer static cylinder. The left sub-panel in figure 1 shows streamlines of the streamwise-averaged, instantaneous flow field. One pair of Taylor rolls is observed. The center and right-hand panels show color coded images of the instantaneous stream-wise velocity component u_θ and the spanwise velocity component u_y, respectively.

In Figure 2, the mean velocity $\overline{\mathbf{U}}(r)$ and azimuthal turbulent intensity $\overline{\mathbf{u}'\mathbf{u}'}$ are shown. All profiles are scaled using the inner viscous velocity $u_{\tau i}$, with $U^+ \equiv \overline{U_\theta}/u_{\tau i}$ in figure 2 (top), and $(u'_\theta u'_\theta)^+ \equiv \overline{u'_\theta u'_\theta}/u^2_{\tau i}$, $(u'_y u'_y)^+ \equiv \overline{u'_y u'_y}/u^2_{\tau i}$ and $(u'_r u'_r)^+ \equiv \overline{u'_r u'_r}/u^2_{\tau i}$ in figure 2 (bottom), versus the scaled length $r^+ = (r - r_i)/l^+$ with $l^+ = \nu/u_{\tau i}$. The present LES mean-velocity profile is found to agree quite well with the direct numerical simulation by Ostilla-Mónico *et al.* (2016). A clear log variation is evident in the $U^+ - r^+$ plot.

Further comparison with DNS at $Re_i = 3 \times 10^5$ is shown in figure 3. The mean-velocity and turbulence intensities obtained from the wall-resolved LES with $(N_\theta, N_r, N_y) = (512 \times 512 \times 768)$, also shows satisfactory comparison with DNS.

4 Discussion

4.1 Mean profiles

As shown for TC flows at $Re_i = 10^5$ and 3×10^5, the log-variation in the velocity profile U^+ in TC flow persists only in a range of r^+. When r^+ is relatively large, meaning close to the center, the profile deviates substantially from the log law. This can be attributed to the strong spanwise redistribution effect produced by Taylor vortices which results in an almost constant angular momentum. In the estimate

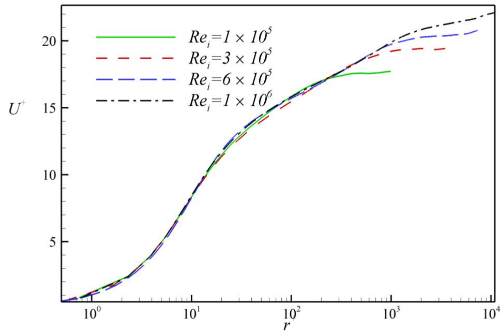

Figure 4. Mean velocity profile for all present LES.

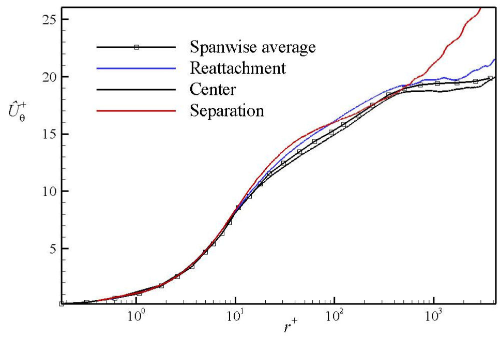

Figure 5. Time and azimuthal averaged velocity profile $\widehat{U}_\theta^+$ at different spanwise locations for $Re_i = 3\times10^5$.

of Ostilla-Mónico *et al.* (2016), $r^+ = 0.1Re_\tau$ is considered as an upper bound for the log layer for case of $\eta = 0.909$.

Mean velocity profiles $U^+(r^+)$ obtained from LES at higher Re_i are shown in figure 4 for the four cases implemented. At $Re_i = 10^6$ the log layer appears to persist up to about $r^+ = 1500$, which is roughly 15% of corresponding Re_τ. In the present LES, an estimate of the Kármán constant κ was obtained using a best-fit log profile to the LES data over a window in R^+ of the calculated mean-velocity profiles. From our two highest Re_i we obtain $\kappa \approx 0.40$, which is consistent with DNS at Re_i up to 3×10^5.

4.2 Span-wise distribution

It is also interesting to investigate the time and azimuthal averaged velocity profiles at different spanwise locations. In the time and azimuthal averaged flow fields, the Taylor roll structure is stationary. We choose three typical positions in the spanwise direction relative to the Taylor rolls. On the inner cylinder surface, we can locate a separation point and a reattachment point as depicted in the left-hand panel of figure 1. We also choose the spanwise coordinate at the location of the center of the Taylor roll, shown at about $y/d = 0.55$ in figure 1. For these three locations, we plot the scaled velocity profiles $\widehat{U}_\theta^+ = \widehat{U}_\theta/u_{\tau i}$ for $Re_i = 3\times10^5$ in figure 5, with comparison to the mean velocity profile U^+. Two velocity $\widehat{U}_\theta^+$ profiles, at the reattachment point and at the center point, show a somewhat similar r^+ variation to that of the mean profile $U^+(r^+)$. The exception is the velocity profile obtained at the spanwise separation point. Here the velocity profile shows a continued increasing tendency along the r direction. Unlike the other profiles, a strong deficit off the log layer is not observed .

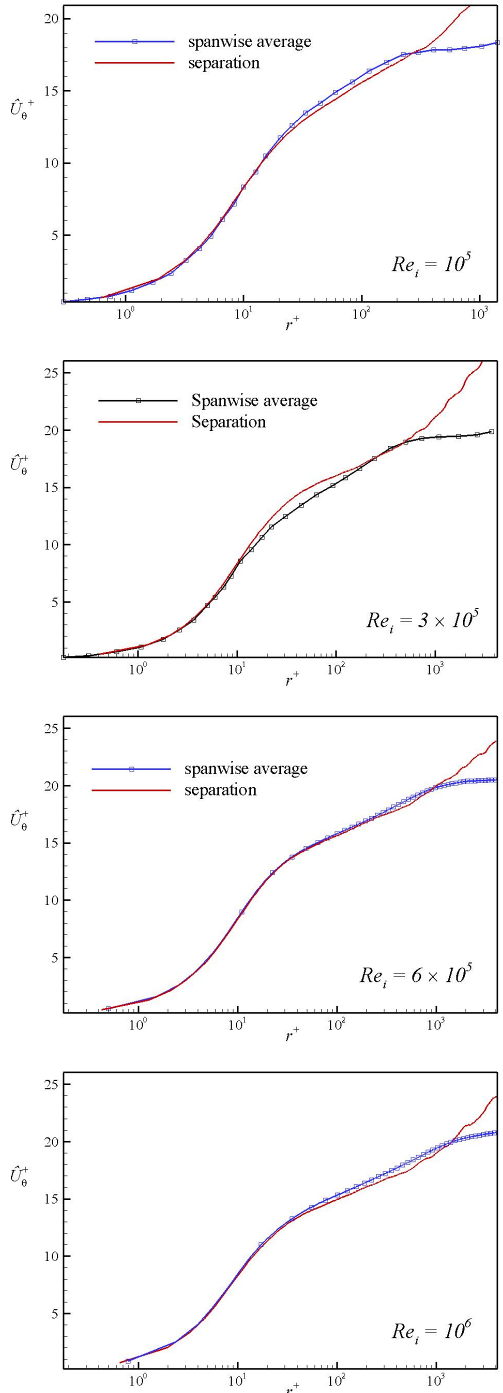

Figure 6. Time and azimuthal averaged velocity profiles $\widehat{U}_\theta^+$ at the separation point for $Re_i = 10^5$, 3×10^5, 6×10^5 and 10^6.

To check the behavior at different Re_i, we compare $\widehat{U}_\theta^+$ at the separation point and U^+ for all four cases in figures 6. It is clear that for all cases, the tendency for continued increase in $\widehat{U}_\theta^+$ beyond the log-layer region persists almost up to its corresponding maximum value of r^+, which equals to Re_τ.

Conclusion

The present study uses wall-resolved large-eddy simulation (LES) to simulate Taylor-Couette flow with a narrow gap (radius ratio $\eta = r_i/r_o = 0.909$) between the inner, rotating cylinder and the outer stationary cylinder. The cases are implemented via a general curvilinear coordinate code with a fully staggered velocity mesh. Fourth-order central difference schemes are used for all spatial discretization. The stretched-spiral vortex SGS model is implemented on the η cell face which minimize the boundary condition effect of the SGS terms.

Two cases at $Re_i = 10^5$ and 3×10^5 are used as verification cases. By comparing mean velocity profile U^+ and turbulent intensities $(u'_\theta u'_\theta)^+$, $(u'_y u'_y)^+$ and $(u'_r u'_r)^+$, we show that the present LES framework can reasonably capture the salient features of TC flows, including the quantitative behavior of spanwise Taylor rolls, the log profile in the mean velocity profile and the angular momentum redistribution due to the presence of Taylor rolls.

Our higher Re_i LES also show strong redistribution effects due to the Taylor vortices. An interesting phenomenon is that, for the azimuthal and time averaged velocity field, the azimuthal velocity profile at a spanwise location corresponding to the mean-flow separation line/point shows different behavior in comparison to profiles at other spanwise locations. This "separation-point" profile is found to consistently increasing along the r direction with the effect that the angular momentum redistribution effect is not significant. This phenomenon is observed in all present cases.

Acknowledgement

The Cray XC40 Shaheen at KAUST was used for all simulations reported.

REFERENCES

Chung, D. & Pullin, D. I. 2009 Large-eddy simulation and wall modelling of turbulent channel flow. *J. Fluid Mech.* **631**, 281–309.

Grossmann, S., Lohse, D. & Sun, C. 2016 High-Reynolds number Taylor-Couette turbulence. *Annual Review of Fluid Mechanics* **48** (1), 53–80.

Lundgren, T. S. 1982 Strained spiral vortex model for turbulent fine structure. *Phys. Fluids* **25** (12), 2193–2203.

Misra, A. & Pullin, D. I. 1997 A vortex-based subgrid stress model for large-eddy simulation. *Phys. Fluids* **9** (8), 2443–2454.

Morinishi, Y., Lund, T.S., Vasilyev, O.V. & Moin, P. 1998 Fully conservative higher order finite difference schemes for incompressible flow. *Journal of Computational Physics* **143** (1), 90–124.

Ostilla-Mónico, R., Verzicco, R., Grossmann, S. & Lohse, D. 2016 The near-wall region of highly turbulent Taylor-Couette flow. *Journal of Fluid Mechanics* **788**, 95117.

Ostilla-Mónico, R., Verzicco, R. & Lohse, D. 2015 Effects of the computational domain size on direct numerical simulations of Taylor-Couette turbulence with stationary outer cylinder. *Physics of Fluids* **27** (2), 746–325.

Pirozzoli, S., Bernardini, M. & Orlandi, P. 2014 Turbulence statistics in Couette flow at high Reynolds number. *Journal of Fluid Mechanics* **758**, 327–343.

Taylor, G. I. 1923 Stability of a viscous liquid contained between two rotating cylinders. *Philosophical Transactions of the Royal Society of London Series A* **223**, 289–343.

Voelkl, T., Pullin, D. I. & Chan, D. C. 2000 A physical-space version of the stretched-vortex subgrid-stress model for large-eddy simulation. *Phys. Fluids* **12**, 1810–1825.